Journal of Innate Immunity

Research Article

J Innate Immun 2025;17:176–197
DOI: 10.1159/000543244

Received: January 29, 2024
Accepted: December 16, 2024
Published online: March 13, 2025

CAPN1 Promotes *Pseudomonas aeruginosa*-Induced Infection by Interacting with TFEB and Inhibiting Autophagy

Yueming Wu[a] Miaomiao Chen[a] Hua Chen[a] Liuhua Pan[a] Jing Zhao[a] Shunnan Sun[a] Ning Zhang[b] Junlong Xu[a]

[a]Department of Critical Care Medicine, The Six Affiliated Hospital of Wenzhou Medical University, Lishui, China;
[b]Department of Emergency Medicine, The Six Affiliated Hospital of Wenzhou Medical University, Lishui, China

Keywords
Acute lung injury · CAPN1 · TFEB · Autophagy-lysosome pathway

Abstract
Introduction: Autophagy-lysosome pathways play a crucial role in the intracellular killing of pathogenic microorganisms. This study aimed to explore the mechanism by which acute lung injury (ALI) of *Pseudomonas aeruginosa* affects the autophagy-lysosome pathway. ***Methods:*** ALI mouse models were induced by lipopolysaccharide and *P. aeruginosa* strain K (PAK). Lung tissue sections were stained with hematoxylin-eosin for observation. Flow cytometry was used to analyze bacteria and inflammatory cell infiltration. ELISA was performed to measure inflammatory factor levels. Transmission electron microscopy evaluated autolysosome quantity. Western blot detected levels of related proteins. Immunofluorescence evaluated LC3 expression, and the localization of TFEB in cells was observed. Co-immunoprecipitation and pull-down experiments confirmed the interaction between CAPN1 and TFEB. qRT-PCR measured *capn1* and *tfeb* expression. ***Results:*** Mouse experiments revealed that PAK infection led to the suppression of autolysosomes in mouse lung tissue, along with increased CAPN1 expression and decreased TFEB in the lung tissue of PAK-induced pneumonia mice. CAPN1-deficient mice could reverse the impact of PAK infection on autolysosomes in mouse lung tissue. These findings were further verified by cell experiments. At a mechanistic level, CAPN1 can interact with TFEB after PAK infection and prevent its entry into the nucleus, thereby inhibiting the autophagolysosomal pathway. ***Conclusion:*** CAPN1 promotes PAK-induced ALI by inhibiting the autophagy-lysosome pathway by targeting TFEB.

Introduction

Acute lung injury (ALI) and acute respiratory distress syndrome (ARDS) represent significant global public health challenges. Infections from viruses and bacteria continue to be a leading cause of mortality related to infectious diseases [1]. *P. aeruginosa*, a common pathogen in hospital-acquired pneumonia, is recognized for its role in causing severe acute and chronic lung infections [2, 3]. *P. aeruginosa* infection leads to the death of pulmonary epithelial cells, disrupting the integrity of the air-blood barrier and

Yueming Wu and Miaomiao Chen contributed equally to this work.

karger@karger.com
www.karger.com/jin

Correspondence to:
Ning Zhang, ningzhang789@163.com
Junlong Xu, xujunlong0927@163.com

causing leakage and edema. This process triggers the recruitment of neutrophils, macrophages, and lymphocytes from the bloodstream, intensifying the inflammatory response [4]. With limited effective treatment options available, the prognosis for patients with ALI/ARDS resulting from *P. aeruginosa* infection remains grim [5]. Therefore, comprehending the molecular mechanisms of lung injury induced by *P. aeruginosa* is essential for devising improved strategies to prevent ALI and ARDS and decrease patient mortality.

Protein toxicity and oxidative stress are key factors in lung inflammation in conditions like sepsis [6], making autophagy a focal point in recent research on ALI. Autophagy serves as a vital antioxidant pathway, operating through a complex multi-step process. When cells encounter stressors such as nutrient deprivation (e.g., amino acids or glucose), they trigger signals that induce autophagy. This initiates the formation of a double-membraned structure known as a phagophore within the cytoplasm. The phagophore expands, enveloping cellular components or autophagic cargo to form a sealed autophagosome. These autophagosomes then merge with lysosomes to create autolysosomes, where lysosomal enzymes break down the contents of autophagosomes. The resulting degradation products are recycled by the cells [7]. Given that autolysosomes play a pivotal role in clearing pathogenic microorganisms within cells, preventing autolysosome dysfunction emerges as a crucial strategy for combating lung infections and immune suppression [8, 9]. Zhang et al. [10] found that autophagy plays a protective role in ischemia-reperfusion injury-induced ALI, and the ERK1/2 signaling pathway has a positive regulatory role in ALI caused by ischemia-reperfusion injury. The study by Ceelen et al. [11] indicated an increased LC3B-II/I ratio, decreased ULK1 phosphorylation, and elevated Gabarapl, Bnip, and p62 mRNA levels in emphysematous mice, providing evidence of autophagy-lysosome pathway (ALP) activation in skeletal muscles following lung inflammation. Yet, there is a lack of comprehensive information concerning the effects of *P. aeruginosa* strain K (PAK) infection on the ALP in PAK-induced ALI.

CAPN1, a member of the Calpain family, along with its counterparts, is responsible for orchestrating the controlled breakdown of a wide range of substrate proteins [12]. In normal physiological conditions, calpains play roles in diverse cellular activities such as restructuring the cytoskeleton, modulating signaling pathways, activating platelets, facilitating cell differentiation, and regulating apoptosis [13, 14]. When CAPN1 is excessively activated, it can lead to uncontrolled protein degradation and abnormal activation of signaling pathways, causing cellular damage and eventual cell death [15]. Previous studies have linked calpains to apoptotic cell death, tissue injury, and their significant involvement in regulating inflammatory responses [16, 17]. Yamashima and others [18, 19] have proposed that CAPN activation induced by brain ischemia promotes lysosomal membrane permeabilization and the release of lysosomal proteases into the cytoplasm, triggering lysosomal protease-dependent cell apoptosis. Recent research has also indicated that CAPN1 activation-mediated autophagy-lysosomal pathway (ALP) features in neuronal damage induced by brain ischemia, suggesting that CAPN1 activation impairs lysosomal function, inhibiting the ALP and exacerbating neuronal damage after brain ischemia [20]. However, it is yet to be determined whether CAPN1 demonstrates a comparable reaction within the ALP in ALI.

In conclusion, understanding the potential molecular mechanisms of ALI is crucial for the development of novel therapeutic approaches for ALI patients. This study explored the specific mechanisms by which CAPN1 affected ALI in PAK-induced mouse models, and we found that CAPN1 can interact with TFEB and prevent its entry into the nucleus, thereby inhibiting the autophagy-lysosomal pathway and thus promoting PAK-induced ALI. This suggested that targeting autophagy-lysosome signal transduction might be a potential avenue for ALI treatment.

Materials and Methods

Bioinformatics Analysis

Transcriptomic data for sepsis were supplied with the Gene Expression Omnibus database (https://www.ncbi.nlm.nih.gov/geo/). The dataset, with accession number GSE123729 and platform number GPL21970, included "control" ($n = 11$) and "sepsis" ($n = 15$) samples. Pearson correlation analysis was conducted to assess the linkage between *capn1* and *tfeb* expression.

Cell Culture and Transfection

The TC-1 cell line (BFN60805941) was obtained from Shanghai Cell Bank (China) and kept in RPMI-1640 medium (Gibco, USA), containing 10% fetal bovine serum (Sigma, USA) and 1% double antibiotics (penicillin and streptomycin) at 37°C in a 5% CO_2 atmosphere. si-NC and si-*capn1* sequences were designed and synthesized in RiboBio (China). oe-*tfeb* was constructed using pcDNA3.1 plasmid, and empty pcDNA3.1 plasmid was used as oe-NC. The plasmid was purchased from Hanbio

Table 1. Primer sequences

Gene	Primer sequence	
CAPN1	Forward primer	5′-CCGTGGACTTTGACAACTTTG-3′
	Reverse primer	5′-CCCCACTTCAGGCAAACATAG-3′
TFEB	Forward primer	5′-CTACATATCAGCTCCAACCCC-3′
	Reverse primer	5′-ACCGCTGTACACGTTCAG-3′
β-actin	Forward primer	5′-GAAGCTGTGCTATGTTGCTCTA-3′
	Reverse primer	5′-CAATAGTGATGACCTGGCCGT-3′

Technology (China). According to the manufacturer's protocol, plasmids and siRNAs were transfected into TC-1 cells with Lipofectamine 2000 (Thermo Fisher Scientific, USA) for 48 h, respectively, and subsequent experiments were conducted.

PAK Cultivation

PAK was obtained from the China Center of Industrial Culture Collection and stored in the culture preservation box at 4°C by semi-solid preservation method. For bacterial revival, a small number of bacteria were directly picked from the culture tube and streaked onto a regular agar plate or into a meat broth tube, followed by incubation at 37°C for 18–24 h.

ELISA

0.5 mL PBS was dribbled into the trachea of mice and lavage repeated for 3 times. Then, the mice's bronchoalveolar lavage fluid (BALF) was collected. The collected BALF and cell culture medium were centrifuged at 3,000 rpm/min for 20 min, and the supernatant was collected for the detection of TNF-α, IL-1β, and IL-6 levels. Specifically, the sample and reaction solution were added in turn according to the kit instructions, mixed, covered with the sealing plate film, and incubated at 37°C for 60 min. After the end, the board was washed with the washing machine 4–5 times, the reaction liquid was added according to the instructions again, incubated at 37°C for 30 min, and the board was washed. Finally, the reaction liquid and the termination liquid were added to each hole according to the instructions, and the OD value of each hole was measured at the wavelength of 450 nm after 10–15 min of hiding from light. All ELISA kits were purchased from Life Technologies (USA).

qRT-PCR

Total RNA was separated using a TRIzol reagent (Invitrogen, USA). To assay mRNA levels of target genes, total RNA was reverse-transcribed into cDNA using a reverse transcription kit (Yeasen, USA). Real-time quantitative PCR was performed using SYBR Green qPCR Mix (Cwbio, China) with the following conditions: 95°C for 10 min, followed by 40 cycles of 95°C for 15 s and 60°C for 1 min. Results were normalized to the level of β-actin. The forward (F) and reverse (R) primer sequences are described in Table 1.

Western Blot

Total protein was isolated from cells using RIPA buffer (Sigma-Aldrich, USA). Subsequently, the proteins were isolated by SDS-PAGE and transferred onto a PVDF membrane, which was blocked with 5% skim milk (Solarbio, China) at room temperature for 2–3 h. Primary antibodies (TFEB, Lamp2A from Huabio, China; LC3B [LC3-II, LC3-I], CAPN1, Lamp2A, CTSD, and β-actin antibodies from ABclonal, China) were incubated with the membrane overnight at 4°C. Subsequently, appropriate secondary antibodies were applied to the membrane at room temperature for 2 h. The secondary antibody for β-actin was goat anti-mouse IgG H&L (HRP), and the others were goat anti-rabbit IgG H&L (HRP). The membrane was washed three times with TBST for 5 min each. ECL Super Sensitive Chemiluminescent Substrate (Yesheng Biological, China) was used for signal detection.

Nuclear Cytoplasmic Fractionation

To determine the effect of CAPN1 expression level on the nucleation of TFEB, the nucleus of TC-1 cells was isolated after transfection by following the instructions of the nuclear/cytoplasmic isolation kit (BioVision, USA). Western blot (WB) experiments were performed using the PARIS™Kit Protein and RNA Isolation System (Invitrogen, USA) to isolate proteins from the nucleus. The WB procedure is the same as that for the TFEB antibody. GAPDH (ab9485) was used as the reference for cytoplasm localization, and Histone H3 was the reference for nuclear localization. Both GAPDH and Histone H3 antibodies were purchased from Abcam (UK).

Hematoxylin-Eosin Staining

Mouse lung tissues were fixed in 4% paraformaldehyde for 6 h, embedded in paraffin, sectioned, and placed in an oven to melt the paraffin. The tissue sections were then deparaffinized into xylene I and xylene II, followed by hydration in a gradient of ethanol (100%, 95%, and 75%). The sections were stained with hematoxylin and eosin, dehydrated in a gradient of ethanol (75%, 95%, 100%, 100%), cleared in xylene I and xylene II, and mounted on coverslips. Cellular morphology was observed using an ML31 biological microscope (mshot, China).

Immunofluorescence Staining

Cell Immunofluorescence

Cells grown on coverslips were washed three times with PBS for 5 min each. After fixing with 4% paraformaldehyde, the cells were rinsed with PBS and then subjected to low-temperature antigen retrieval in an EDTA antigen repair solution for 20 min. Following three rinses with PBS, the cells were permeabilized with 0.1% Triton X-100 and subjected to additional PBS washes. Subsequently, they were blocked with 5% milk for 30 min and exposed to a primary antibody (LC3, sourced from Proteintech, China) or (TFEB, sourced from ABclonal, China) for overnight incubation at 4°C. After incubation with a goat anti-rabbit secondary antibody conjugated with Alexa Fluor 555 (Beyotime, China) for 60 min, cell nuclei were stained with DAPI (Beyotime, China) for 2–3 min. Sample observation was done using a fluorescence microscope (Leica Microsystems, USA).

Animal Lung Tissue Immunofluorescence

Mouse lung tissues were fixed in 4% paraformaldehyde for 6 h, embedded in paraffin, and sectioned (4 μm). After deparaffinization and antigen retrieval in EDTA antigen repair solution, the sections were blocked with peroxidase blocking solution at room temperature for 10 min, followed by three PBS washes for 5 min each. The sections were then blocked with 5% milk at 37°C for 30 min and kept at 37°C for 90 min with a primary antibody (LC3, from Proteintech, China). Subsequently, the sections were incubated at 37°C for 30 min with a goat anti-rabbit secondary antibody conjugated with FITC (Beyotime, China). Cell nuclei were stained with DAPI for 5 min. Sample observation was carried out using a fluorescence microscope (Leica Microsystems, USA).

Transmission Electron Microscopy

Tissues or cells were submerged in a 30 mM HEPES buffer (pH 7.4) at 4°C and underwent fixation with 2% PFA and 2% glutaraldehyde for 30 min. This was succeeded by a 1% osmium tetroxide fixation for 1 h. Following a process of dehydration using a series of graded ethanol solutions, the samples were subsequently embedded in epoxy resin. Ultra-thin sections were stained with 1% uranyl acetate for 30 min and then with Reynolds' lead citrate for 5 min. Finally, samples were observed for autolysosome morphology using a Hitachi H-7650 electron microscope (Japan).

Flow Cytometry for Assessment of Inflammatory Cell Infiltration in BALF

To prevent nonspecific binding of immunoglobulins to Fc receptors, rat anti-mouse CD16/CD32 antibodies (BD Biosciences, USA) were added to the BALF sample. A strict gating strategy was employed to differentiate between different immune cell populations, and dead cells were excluded using propidium iodide. Neutrophils and macrophages were gated based on their medium-to-high forward scatter (FSC-A) and side scatter (SSC-A) characteristics, which were distinct from lymphocytes and bone marrow cells. Neutrophils were classified as $CD45^{Hi}$, $CD66a^{Hi}$, and $Ly6G^{+}$, while macrophages were classified as $CD45^{Hi}$, $F4/80^{Hi}$, and $Ly6G^{-}$. Different subsets of macrophages included alveolar macrophages ($CD11b^{low}$, $CD11c^{Hi}$), exudative macrophages ($CD11b^{Hi}$, $CD11c^{Hi}$), and infiltrating macrophages ($CD11b^{Hi}$, $CD11c^{Low}$). The cells were analyzed on an Agilent NovoCyte flow cytometer (Agilent, USA), and the data were analyzed using FlowJo software (FlowJo LLC, USA). The antibodies used included FITC-conjugated CD45 antibody, PE/Cy7-conjugated CD11c antibody, APC-conjugated CD11b antibody, APC/Cy7-conjugated Ly6G antibody, all of which were purchased from BD Biosciences (USA), and APC-conjugated CD66a antibody purchased from BioLegend (USA).

Animal Experiments

Nine 4-week-old male C57BL/6 mice were obtained from the Zhejiang Experimental Animal Center and were kept under standard conditions with a temperature of approximately 22°C, humidity at 50%, and a 12-h light-dark cycle. The mice were randomly divided into three groups, each containing 3 mice.

1. Lipopolysaccharide (LPS) Group: Anesthesia was induced in the mice using 3% isoflurane, and they were secured to an operating table. The trachea was surgically exposed along the midline of the neck, and LPS (3 mg/kg) was administered to the trachea by intubation. After intubation, the mice were positioned vertically and rotated to ensure even distribution of the drug in the lungs. The survival rate of the mice was 100%.

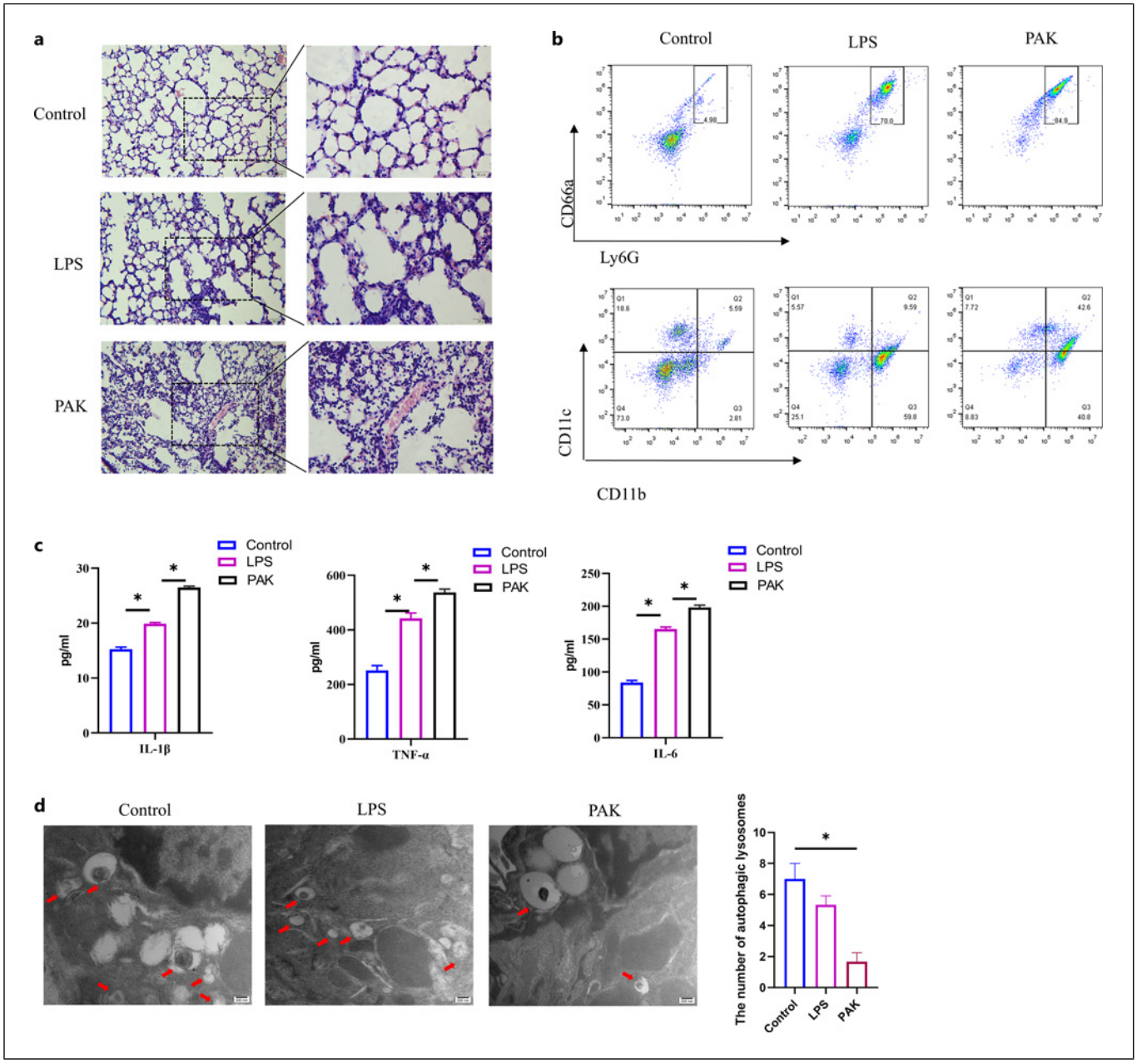

1

(Figure continued on next page.)

2. Control Group: The mice received tracheal instillation of saline as a control. The survival rate of the mice was 100%.
3. PAK Group: PAK was cultured on LB agar plates for 16 h, and the colonies were resuspended in sterile saline. Anesthesia was induced in the mice, and they received 50 μL (1×10^7 CFU) of PAK via intratracheal instillation. The survival rate of the mice was 100%. The mice were euthanized 6 h after PAK treatment and 12 h after LPS treatment, and lung tissue homogenates and BALF were collected for further analysis. Each group contained 3 mice. All experimental procedures were approved by the Experimental Animal Ethics Committee of Lishui University School of Medicine, Approval No. 2023YD0110.

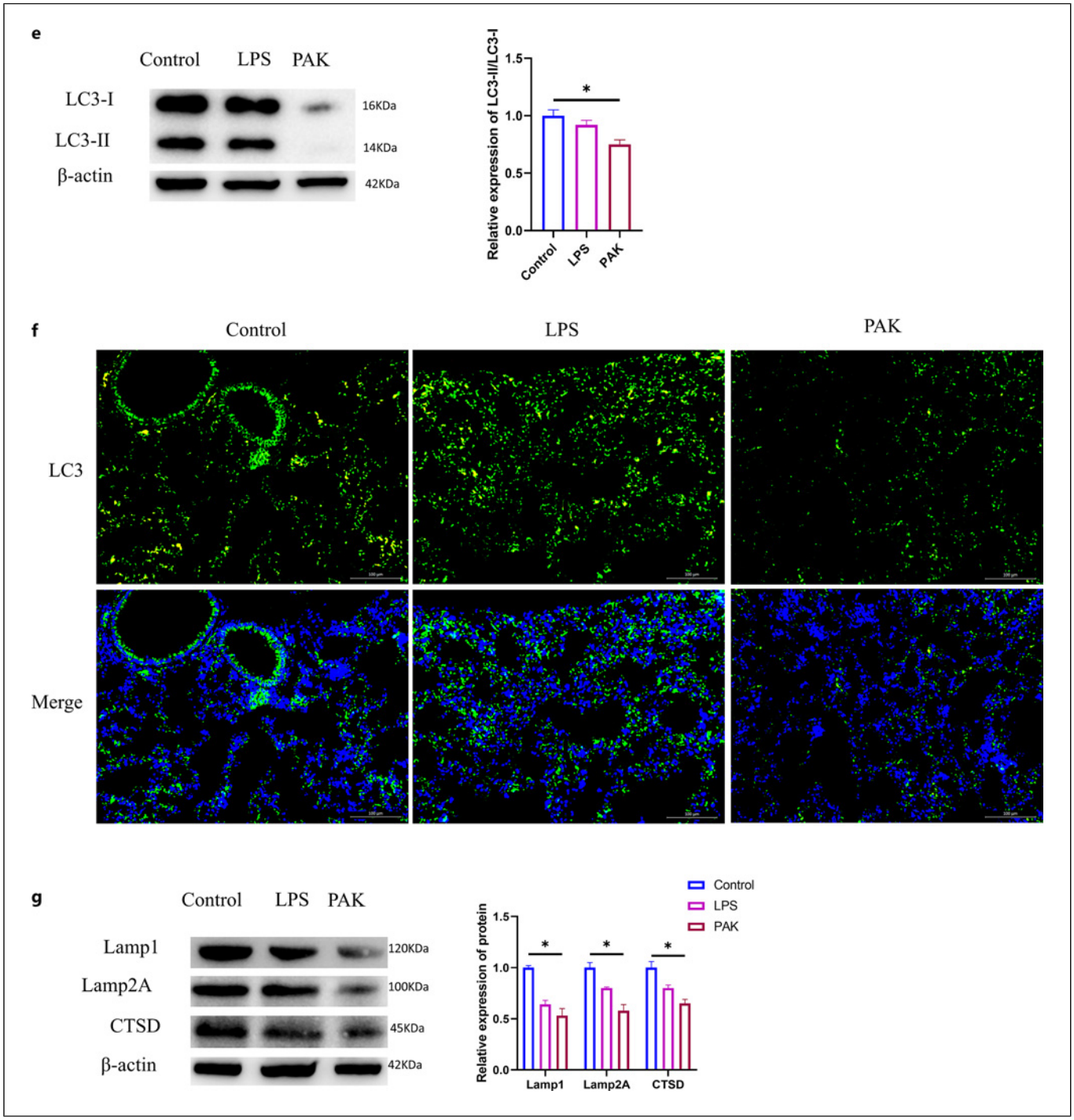

Fig. 1. Autolysosomes are inhibited in the lungs of PAK-infected ALI mice. **a** HE staining was used to observe the effects of LPS and PAK treatment on the degree of alveolar injury in mice, scale bar = 30 μm. **b** Flow cytometry analysis of LPS and PAK treatment on mice alveolar lavage fluid (BALF) in neutrophils ($CD66a^{Hi}$, $Ly6G^{+}$), alveolar macrophages ($CD11b^{Low}$, $CD11c^{Hi}$), exudative macrophages ($CD11b^{Hi}$, $CD11c^{Hi}$), and infiltrating macrophages ($CD11b^{Hi}$, $CD11c^{Low}$) infiltration level. **c** ELISA was used to detect the effects of LPS and PAK treatment on the levels of TNF-α, IL-1β, and IL-6 in BALF. **d** The effects of LPS and PAK treatment on the number of autolysosomes in mouse lung tissue were observed by transmission electron microscopy, scale bar = 200 nm. **e** The effects of LPS and PAK treatment on the expression levels of LC3-II and LC3-I protein in mouse lung homogenate were detected by WB. **f** The effects of LPS and PAK treatments on LC3 expression in mouse lung tissue were detected by IF (Blue, DAPI; Green, LC3), scale bar = 100 μm. **g** The protein expression levels of Lamp1, Lamp2A, and CTSD in lung homogenates treated with LPS and PAK were detected by WB. $n = 3$, * indicates $p < 0.05$. HE, hematoxylin-eosin.

J Innate Immun 2025;17:176–197
DOI: 10.1159/000543244

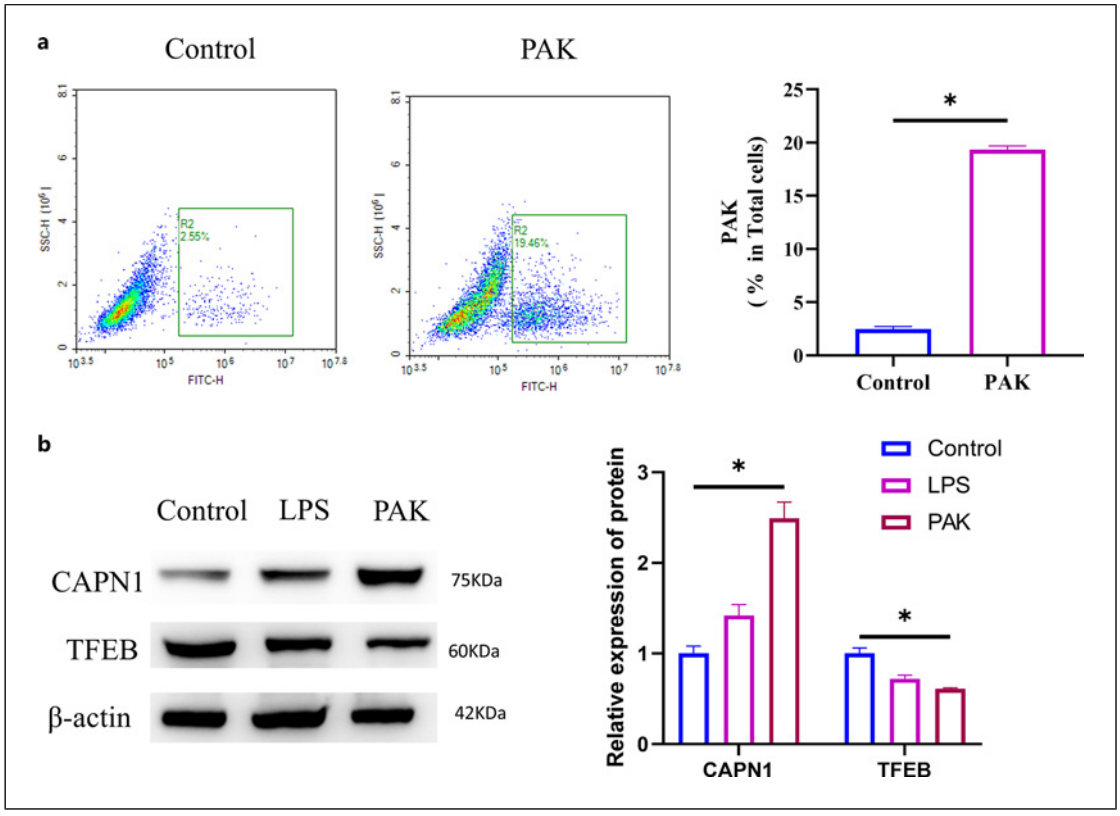

Fig. 2. Elevated expression of CAPN1 and reduced TFEB levels in the lungs of mice induced by PAK. **a** Flow cytometry analysis of bacterial load in mouse tissues following PAK infection. **b** The effects of LPS and PAK treatment on the expression of CAPN1 and TFEB protein in mouse lung homogenate were detected by WB. $n = 3$.

Flow Cytometry for Bacterial Load Detection

After PAK infection of C57BL/6 mice for 6 h, lung tissues were collected under sterile conditions. The lung tissues were digested for a certain period (30–60 min) at 37°C in 10 mL RPMI-1640 medium containing 10 mg of type I collagenase (Gibco, USA) and 1 U/mL DNase I (Invitrogen, USA). After digestion, the lung tissues were filtered through a mesh (such as a 70 μm cell strainer) to remove undigested tissue, yielding a cell suspension. The cells were washed with PBS, centrifuged to remove the supernatant, resuspended in a fresh medium to create a cell suspension, and finally analyzed on an Agilent NovoCyte (Agilent, USA).

For both CAPN1 knockout mice (CAPN1−/− mice) and wild-type C57BL/6 mice treated with PAK, cell suspensions were prepared following the same steps as above. The cell suspensions were then separately incubated with Pacific Blue anti-F4/80 (BioLegend, USA) and APC-Cy7 anti-CD31 (BioLegend, USA) for 10 min, followed by analysis using an Agilent NovoCyte (Agilent, USA).

Co-Immunoprecipitation

It was carried out using the Dynabeads Protein G Immunoprecipitation Kit (Thermo Fisher Scientific, USA). In brief, cell lysis was prepared using Pierce IP Lysis Buffer (Thermo Fisher Scientific, USA) supplemented with protease inhibitors (Beyotime Biotechnology, USA). After removing a nonspecific binding to Dynabeads Protein G, an appropriate amount of anti-CAPN1 antibody (Abcam, UK) or anti-TFEB antibody (Abcam, UK), or control IgG (Abcam, UK) was added to the cell lysate and incubated overnight at 4°C. The Dynabeads-Ab-antigen complexes were washed with a washing buffer and eluted using RIPA buffer for subsequent WB analysis.

GST Pull-Down

GST-CAPN1 and His-TFEB plasmids were transfected into TC-1 cells. Approximately 100 μg of GST and GST-CAPN1 fusion proteins were fixed in 50 μL of glutathione agarose beads and equilibrated gently at 4°C for 60 min before use. After being washed three times with PBST,

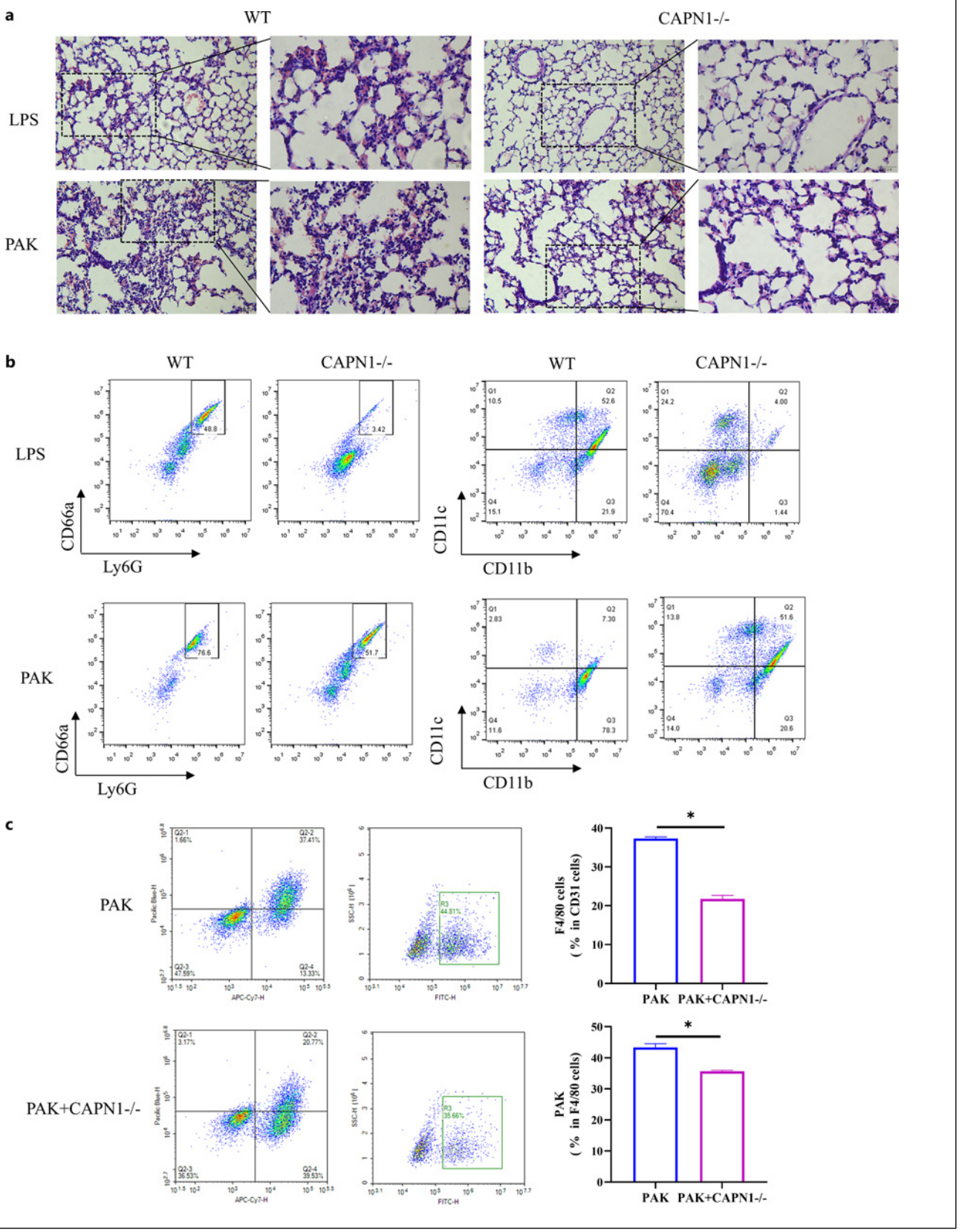

3

(Figure continued on next page.)

J Innate Immun 2025;17:176–197
DOI: 10.1159/000543244

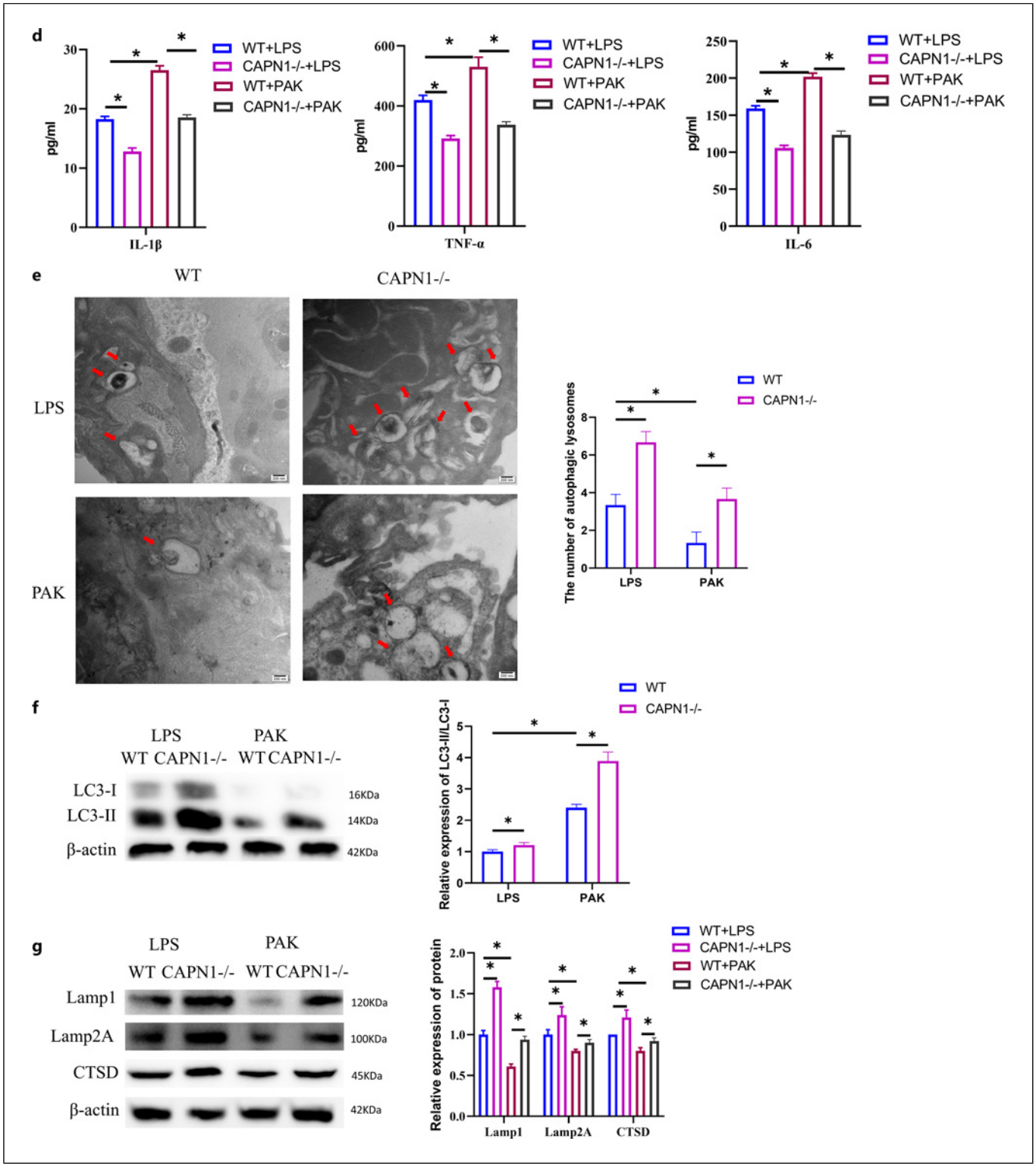

3

(For legend see next page.)

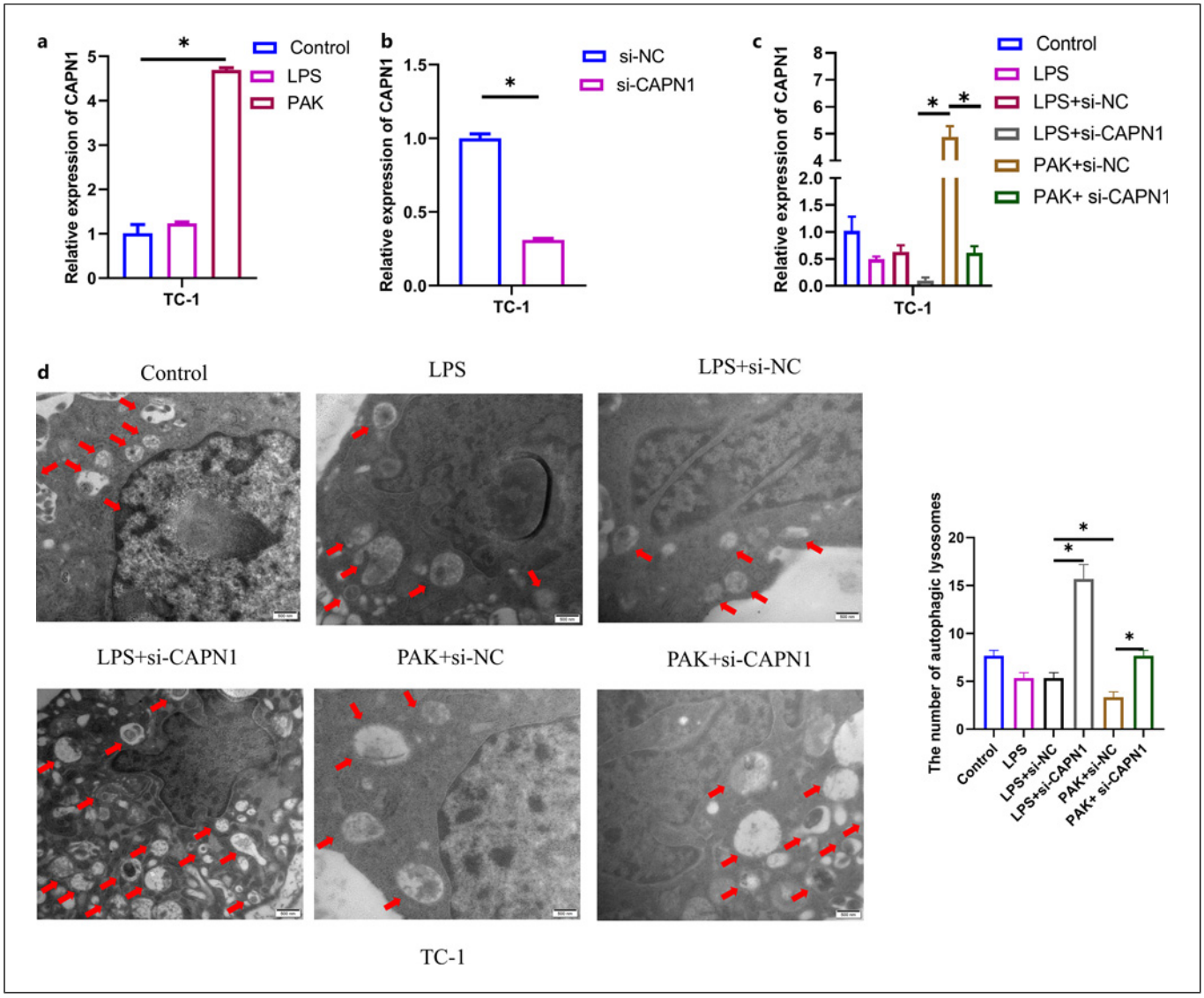

4

(Figure continued on next page.)

approximately 100 μg of His-TFEB fusion protein was added to the fixed GST-CAPN1 and GST. These two fusion proteins were gently mixed and incubated overnight at 4°C. The bound proteins were eluted using elution buffer (10 mM glutathione in PBS, pH 8.0) and analyzed through immunoblotting.

Fig. 3. Effect of CAPN1 knockout on autolysosomes in the lung of PAK-infected ALI mice. **a** HE staining was used to observe the effect of CAPN1 knockout on alveolar damage in LPS and PAK-infected mice, scale bar = 30 μm. **b** Flow cytometry analysis knockout CAPN1 to LPS and PAK-infected mice neutrophils ($CD66a^{Hi}$ $Ly6G^{+}$) in the BALF, alveolar macrophages ($CD11b^{low}$, $CD11c^{Hi}$), exudative macrophages ($CD11b^{Hi}$, $CD11c^{Hi}$), infiltrating macrophages ($CD11b^{Hi}$, $CD11c^{low}$) infiltration level. **c** Flow cytometry analysis of the killing ability of macrophages. **d** ELISA was used to detect the effects of CAPN1 knockout on TNF-α, IL-1β and IL-6 levels in LPS and PAK-infected mice in BALF. **e** The effects of CAPN1 knockout on the number of autolysosomes in LPS and PAK-infected mice were observed by transmission electron microscopy, scale bar = 200 nm. **f** The effects of CAPN1 knockout on the expression of LC3-II and LC3-I protein in lung homogenates of LPS and PAK-infected mice were detected by WB. **g** The effects of CAPN1 knockout on the expression levels of Lamp1, Lamp2A, and CTSD in the lung homogenates of LPS and PAK-infected mice were detected by WB. $n = 3$, * indicates $p < 0.05$. HE, hematoxylin-eosin.

J Innate Immun 2025;17:176–197
DOI: 10.1159/000543244

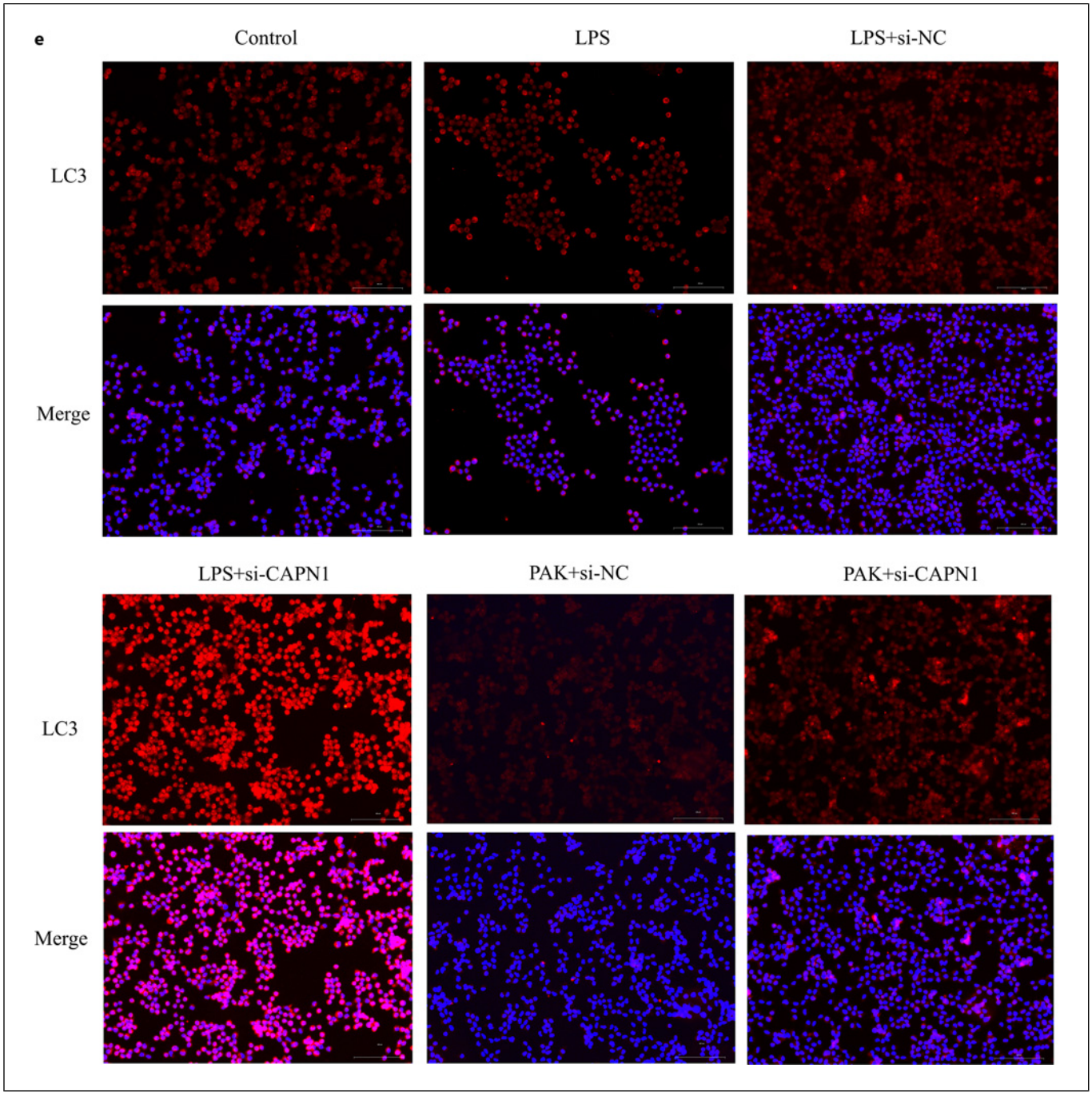

4

(Figure continued on next page.)

Data Analysis

Data were presented as means ± SD. All data were statistically analyzed using GraphPad Prism 6.0 (GraphPad, San Diego, California). Data were processed using *t* tests, one-way or two-way analysis of variance (ANOVA), followed by Dunnett's or Bonferroni's post hoc tests. A significance level of $p < 0.05$ was deemed statistically significant.

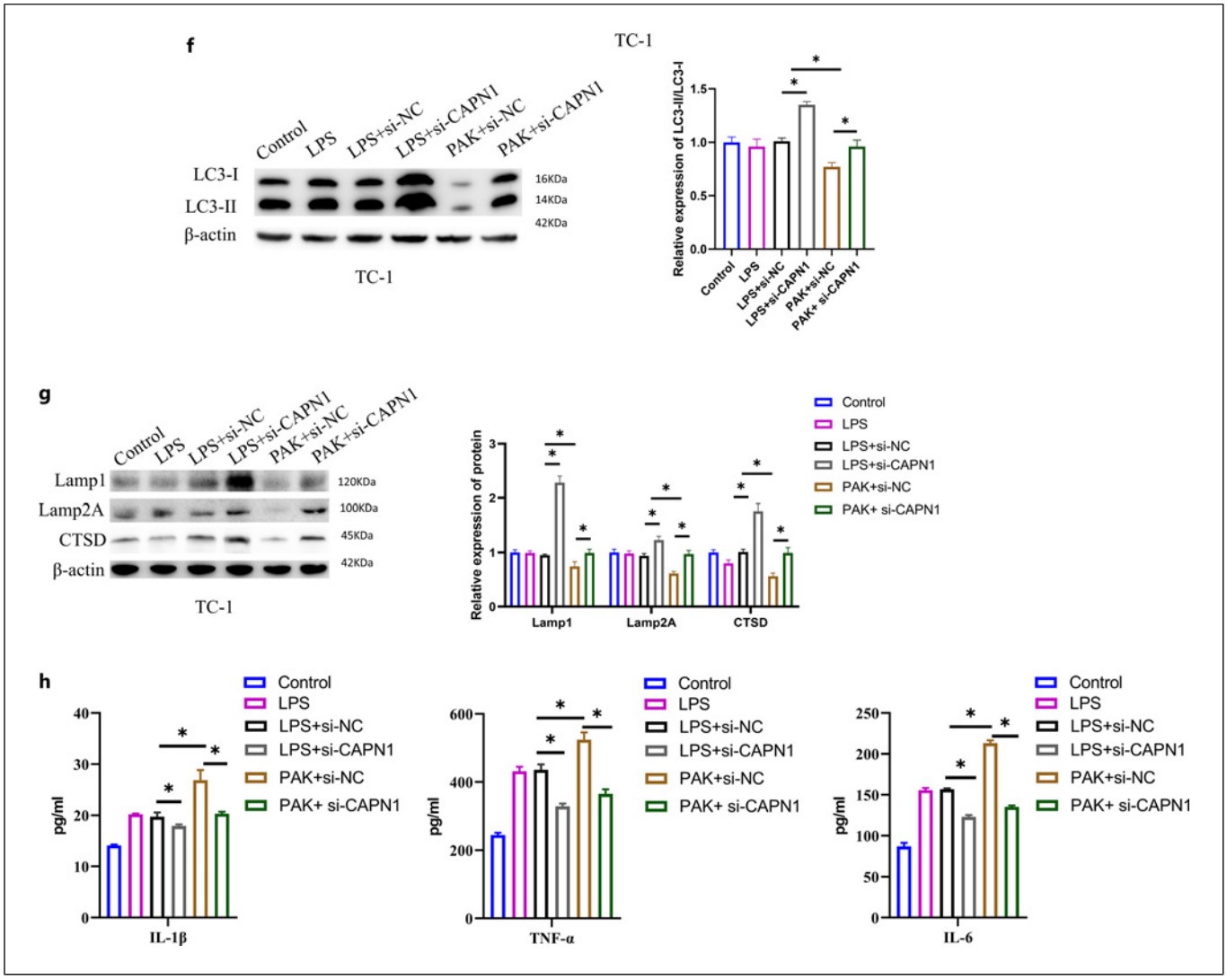

Fig. 4. Effects of CAPN1 on autophagy and inflammatory responses in TC-1 cells infected with PAK. **a–c** mRNA expression of *capn1* in TC-1 cells of different treatment groups was detected by qRT-PCR. **d** The number of autolysosomes in different treatment groups was observed by transmission electron microscopy, scale bar = 500 nm. **e** The expression of LC3 in different treatment groups was detected by IF (Blue, DAPI; Red, LC3), scale bar = 100 μm. **f** The expression levels of LC3-II and LC3-I protein in different treatment groups were detected by WB. **g** The expression levels of Lamp1, Lamp2A and CTSD in different treatment groups were detected by WB. **h** The levels of TNF-α, IL-1β and IL-6 in cell supernatant of different treatment groups were detected by ELISA. $n = 3$, * indicates $p < 0.05$.

Results

PAK Infection Leads to Suppression of the ALP in Mouse Lungs

Considering the pivotal role of autolysosomes in intracellular pathogen elimination, our study sought to elucidate the impact of severe lung infections associated with ALI on the biogenesis of autolysosomes. To assess the effects of aseptic inflammatory conditions and lethal bacterial infections on mouse lung tissue, as well as the levels of phagolysosomes and lysosomes, we established 2 distinct mouse models. One model involved the induction of ALI through LPS administration, simulating aseptic inflammatory conditions, while the control group was treated with saline. The second model entailed the initiation of bacterial-induced ALI using PAK. First, hematoxylin-eosin staining was used to observe lung tissue sections. The results showed that both LPS and PAK treatment caused severe alveolar damage and interstitial edema in mouse lung tissues. The effects were more pronounced in the PAK-treated group

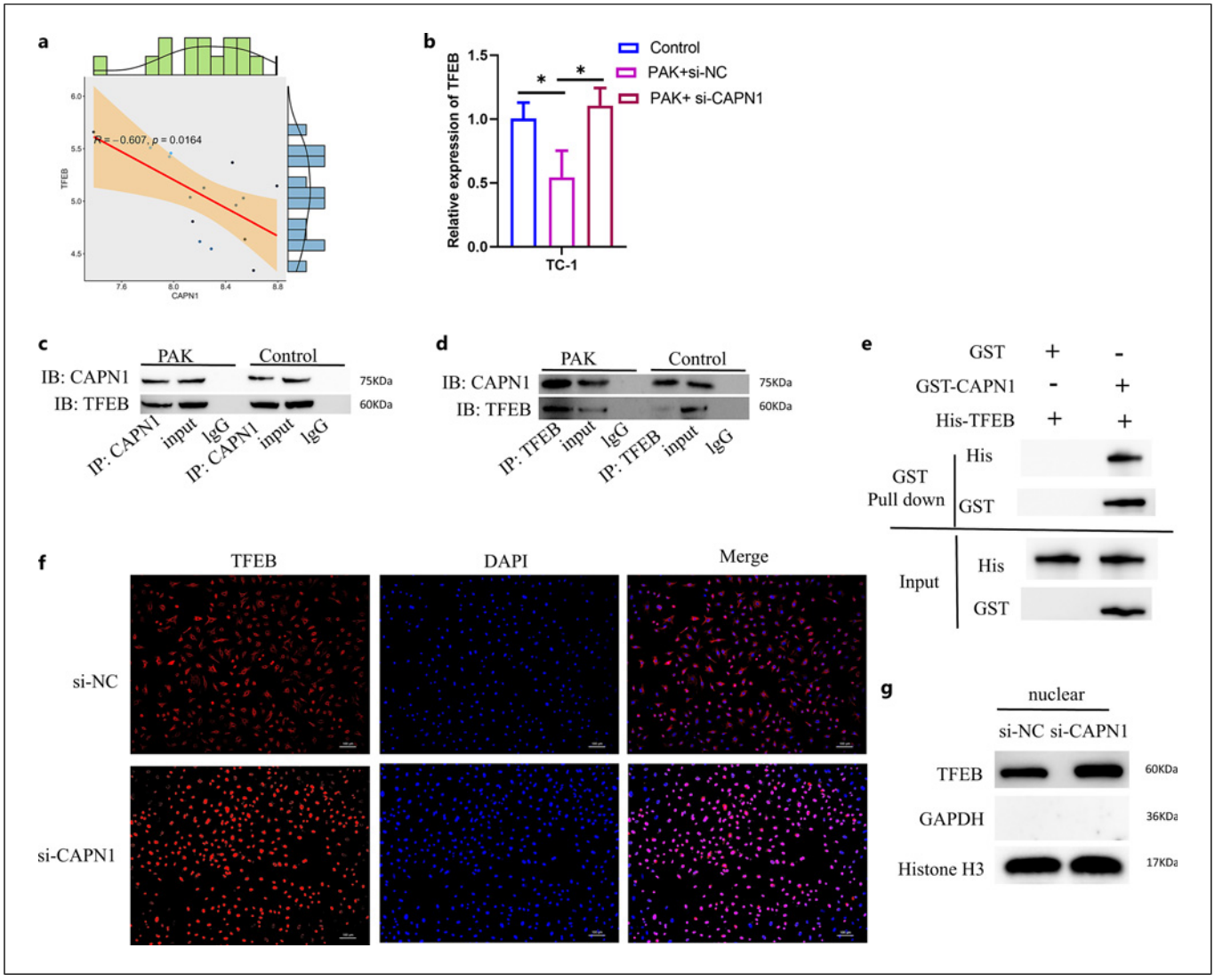

Fig. 5. CAPN1 interacts with TFEB. **a** Pearson correlation analysis was performed for *capn1* and *tfeb*. **b** The mRNA relative expression level of *capn1* in Control, PAK+si-NC, and PAK+si-*capn1* groups was detected by qRT-PCR. **c**, **d** CoIP assay was used to verify the interaction between CAPN1 and TFEB. **e** The pull-down experiment validation of the binding relationship between CAPN1 and TFEB. **f** Localization of TFEB in cells after CAPN1 knockdown was detected by IF (Blue, DAPI; Red, TFEB), scale bar = 100 μm. **g** The effect of CAPN1 knockdown on the expression level of TFEB in the nucleus was detected by WB after karyoplasmic separation. n = 3, * indicates $p < 0.05$. CoIP, co-immunoprecipitation.

(Fig. 1a). Flow cytometry was utilized to analyze the level of inflammatory cell infiltration in BALF. The results indicated that both LPS-induced and PAK-infected mice had increased neutrophil counts in the lungs. Furthermore, analysis of macrophage subpopulations revealed a decrease in alveolar macrophages ($CD11b^{Low}$, $CD11c^{Hi}$) but a significant increase in exudative macrophages ($CD11b^{Hi}$, $CD11c^{Hi}$) and infiltrating monocytes/macrophages ($CD11b^{Hi}$, $CD11c^{Low}$) in the lungs of both LPS-induced and PAK-infected mice. The effect was more pronounced in the PAK-infected group (Fig. 1b). ELISA was used to measure the levels of TNF-α, IL-1β, and IL-6 in BALF. The results showed that both LPS and PAK treatment increased the levels of TNF-α, IL-1β, and IL-6, with the PAK treatment having a more significant effect (Fig. 1c). To investigate the impact of aseptic inflammation and lethal bacterial infection on autolysosomes in the mouse lungs, transmission electron microscopy was used to observe the number of autolysosomes in the tissue. It was found that only PAK infection led to the depletion of autolysosomes

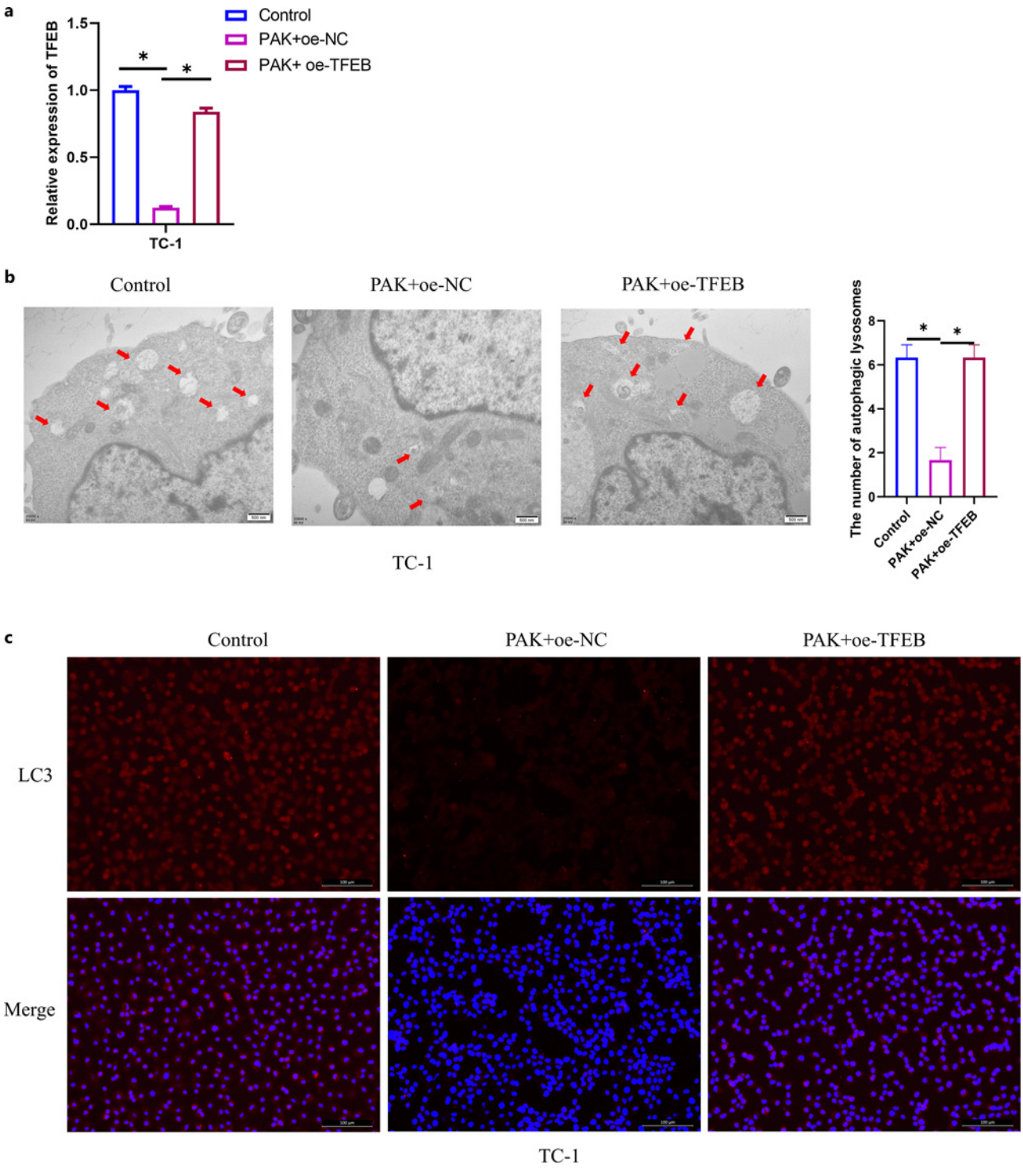

6

(Figure continued on next page.)

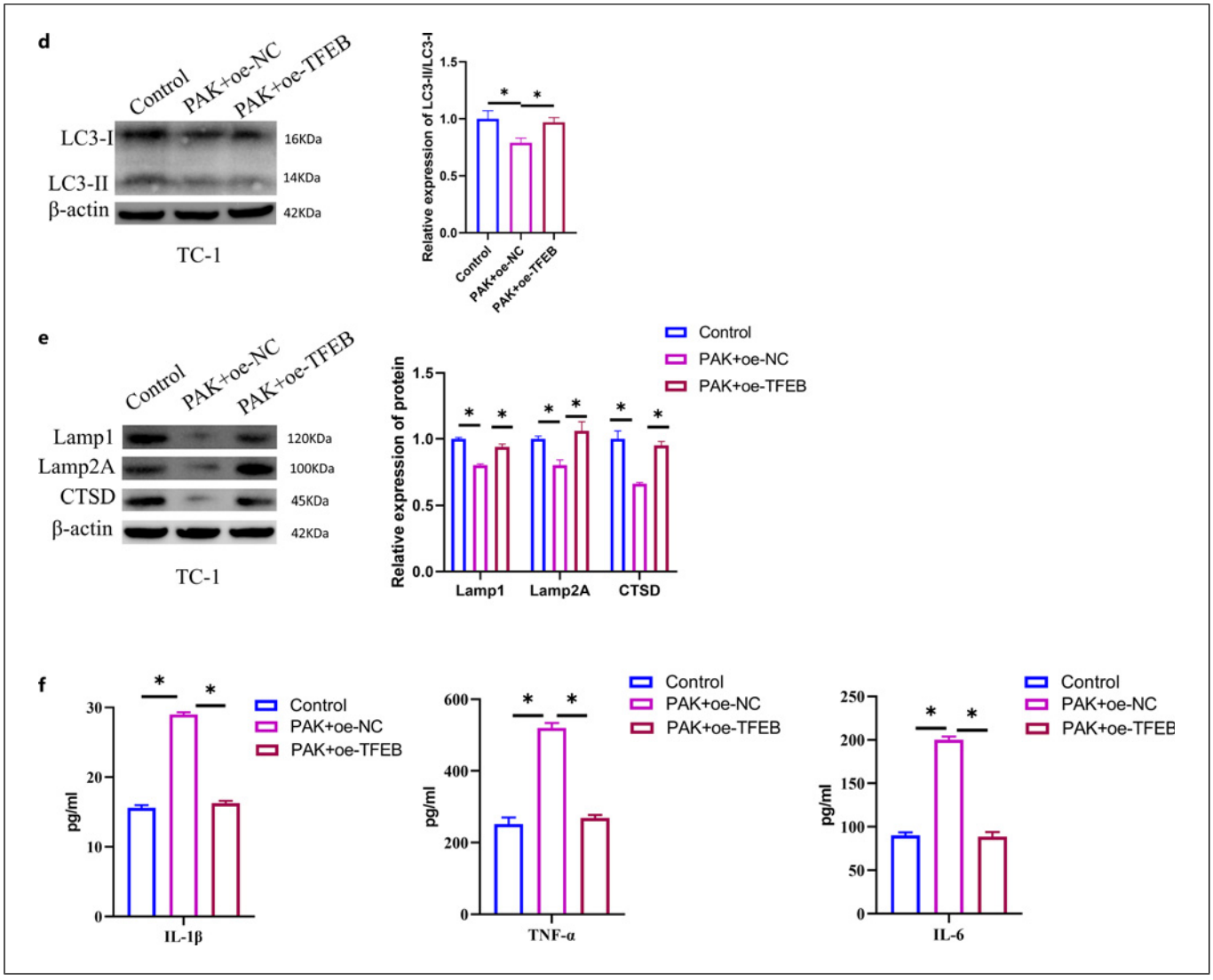

Fig. 6. Effect of TFEB on autophagy and inflammatory responses in PAK-infected TC-1 cells. **a** The relative expression of *tfeb* mRNA in three groups of cells was detected by qRT-PCR. **b** The number of autolysosomes in the three groups of cells was observed by transmission electron microscope, scale bar = 500 nm. **c** The expression level of LC3 in the three groups of cells was detected by IF (Blue, DAPI; Red, LC3), scale bar = 100 μm. **d** The expression levels of LC3-II and LC-I proteins in three groups of cells were detected by WB. **e** The expression levels of Lamp1, Lamp2A, and CTSD in the three groups of cells were detected by WB. **f** The levels of TNF-α, IL-1β, and IL-6 in the supernatant of the three groups of cells were detected by ELISA. $n = 3$, * indicates $p < 0.05$.

(Fig. 1d). WB was used to examine the expression of LC3-II and LC3-I in lung homogenates. Exposure to PAK significantly reduced the LC3-II/LC3-I ratio, while LPS treatment had little or no effect (Fig. 1e). Immunofluorescence (IF) staining for LC3 expression also showed that LPS treatment had a minor impact on LC3 expression, while PAK infection significantly inhibited LC3 expression (Fig. 1f). Furthermore, WB analysis of the expression of lysosome-related membrane proteins Lamp1, Lamp2A, and the protease CTSD in lung homogenates revealed that only PAK infection could suppress the expression of Lamp1, Lamp2A, and CTSD proteins (Fig. 1g). In summary, PAK infection led to the suppression of the ALP in mouse lungs.

Increased Expression of CAPN1 and Reduced Expression of TFEB in PAK-Induced ALI Mouse Lung Tissues

To assess the bacterial load in mice following PAK infection, we used flow cytometry to analyze the quantity of bacteria in mouse tissues 6 h post-PAK infection. The

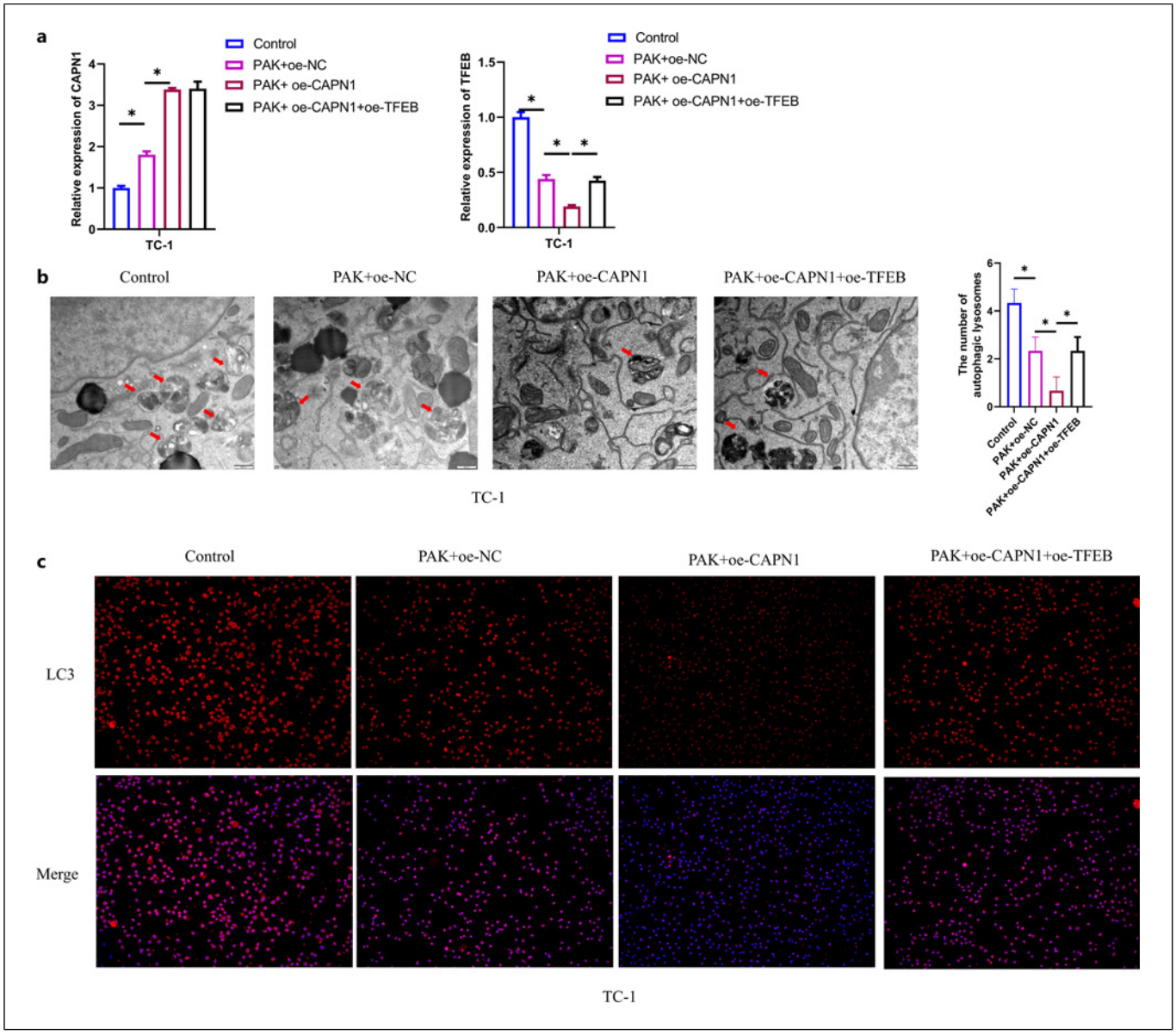

7

(Figure continued on next page.)

results indicated that compared to uninfected mice, there was a significant increase in bacterial content in the lung tissue of mice after PAK infection (Fig. 2a). Previous research has reported elevated expression of CAPN1 in rats with cecal ligation and puncture-induced sepsis [21]. Additionally, CAPN1-mediated autophagic flux impairment leads to neuronal damage in cerebral ischemia-induced injury [20]. TFEB is widely recognized as the "master regulator" of both lysosomal and autophagic pathways due to its role in governing the transcription of numerous genes associated with lysosome biogenesis and the breakdown of autophagic cargo. Moreover, TFEB plays a critical role in nearly every phase of the autophagic process, spanning from autophagosome formation to the degradation of substrates within autophagosomes [22]. Given these observations, it was hypothesized that the suppression of autolysosomes in the lungs of PAK-induced ALI mice might be associated with the expression of CAPN1 and TFEB. Therefore, the expression of CAPN1 and TFEB in lung homogenates from the mouse models was examined, which displayed that only PAK infection induced an increase in CAPN1 expression in

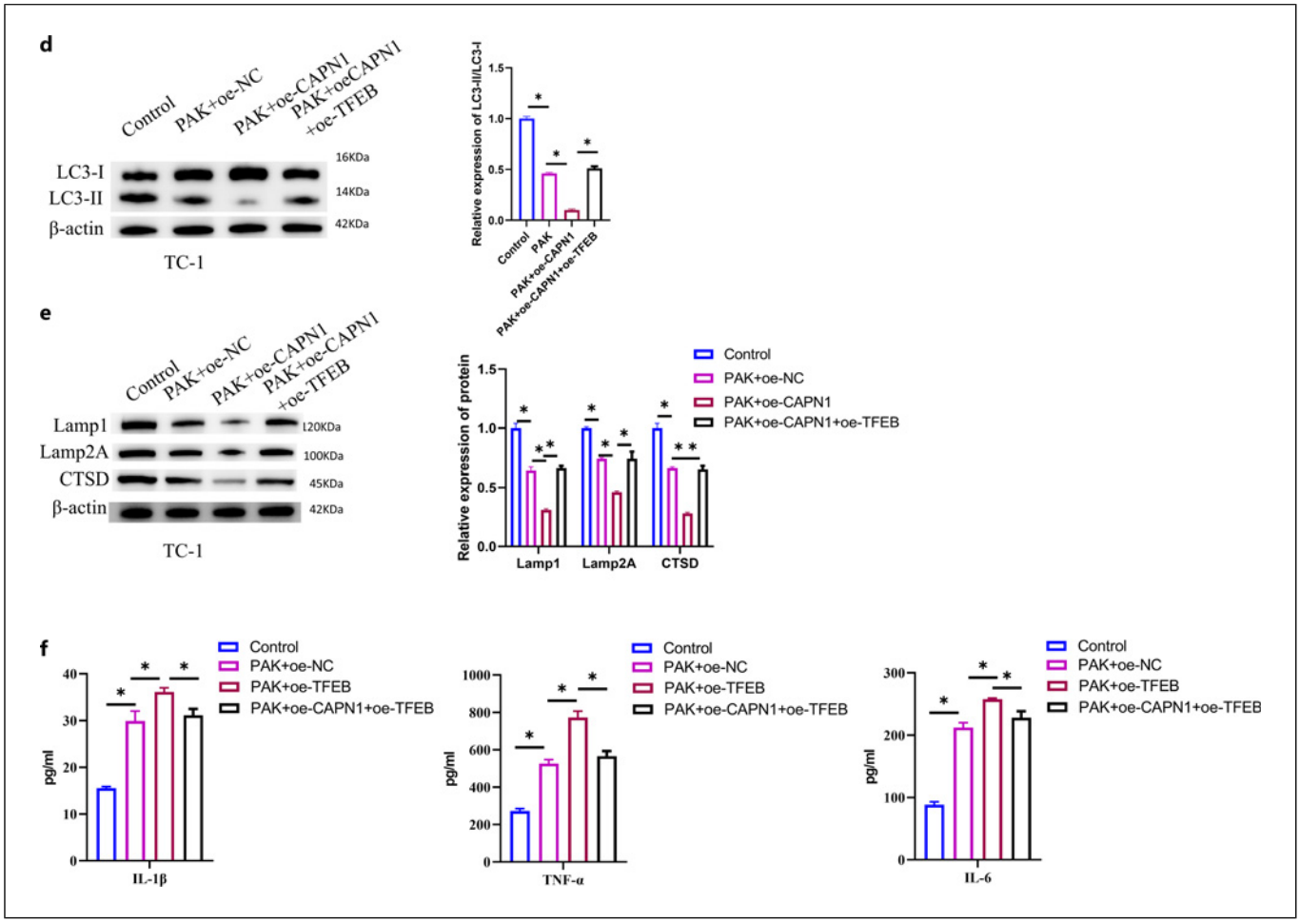

Fig. 7. Effect of CAPN1/TFEB on autophagy and inflammatory responses in PAK-infected TC-1 cells. **a** The relative expression of capn1 and *tfeb* mRNA in four groups of cells was detected by qRT-PCR. **b** The number of autolysosomes in the four groups of cells was observed by transmission electron microscope, scale bar = 500 nm. **c** The expression level of LC3 in the four groups of cells was detected by IF (Blue, DAPI; Red, LC3). **d** The expression levels of LC3-II and LC-I proteins in four groups of cells were detected by WB. **e** The expression levels of Lamp1, Lamp2A, and CTSD in the four groups of cells were detected by WB. **f** The levels of TNF-α, IL-1β and IL-6 in the supernatant of the four groups of cells were detected by ELISA. $n = 3$, * indicates $p < 0.05$.

mouse lung tissue and suppressed the expression of TFEB (Fig. 2b). In conclusion, PAK-induced ALI in mouse lung tissues was linked with an increased expression of CAPN1 and a reduction in TFEB expression.

Impact of CAPN1 Knockout on Autolysosomes in PAK-Infected Mouse Lung Tissues

To investigate the influence of CAPN1 on autolysosomes in mouse lung tissues during ALI, *capn1* knockout mice (*capn1*−/− mice) and wild-type male C57BL/6 mice were obtained and subjected to LPS or PAK treatment. Subsequently, lung tissue pathology was examined through hematoxylin-eosin staining. In the WT group, PAK infection significantly aggravated lung damage compared to LPS treatment. Conversely, in the *capn1* knockout group, lung damage induced by LPS was reduced, and the impact of PAK infection on lung damage in *capn1*−/− mice was restored to control levels (Fig. 3a). The levels of inflammatory cell infiltration in the BALF were analyzed using flow cytometry, with results showing that in the WT mouse group, compared to LPS treatment, PAK infection increased the number of neutrophils and led to a decrease in alveolar macrophages ($CD11b^{Low}$, $CD11c^{Hi}$), but an increase in extravasated macrophages ($CD11b^{Hi}$, $CD11c^{Hi}$) and infiltrating mononuclear cells/macrophages ($CD11b^{Hi}$, $CD11c^{Low}$). However, the effects of PAK on these inflammatory cell infiltration levels were reversed in *capn1*−/− mice (Fig. 3b). The results of flow

cytometry analysis showed that compared to wild-type mice, the bacterial uptake by macrophages in the lung tissue of *capn1*−/− mice was significantly reduced (Fig. 3c). Subsequent ELISA tests were conducted to determine the levels of TNF-α, IL-1β, and IL-6 in BALF, with outcomes showing that, in the WT group, PAK treatment promoted the levels of TNF-α, IL-1β, and IL-6 compared to LPS treatment. Additionally, knocking down *capn1* reduced the LPS-induced release of proinflammatory cytokines compared to the WT group. In *capn1*−/− mice, PAK treatment did not significantly affect the levels of TNF-α, IL-1β, and IL-6 (Fig. 3d). The impact of CAPN1 on autolysosomes in PAK-infected ALI mouse lung tissues was subsequently verified. Transmission electron microscopy revealed that in the WT group, PAK infection led to the depletion of autolysosomes. Nevertheless, this phenomenon was not observed in *capn1*−/− mice (Fig. 3e). WB analysis was performed to assess the expression of LC3-II and LC3-I in lung homogenates. In the WT group, exposure to PAK resulted in a significant reduction in the LC3-II/LC3-I ratio. This effect was mitigated in *capn1*−/− mice (Fig. 3f). Finally, WB analysis was utilized to determine the expression of lysosome-related membrane proteins (Lamp1, Lamp2A) and the protease CTSD in lung homogenates. In the WT group, compared to LPS treatment, PAK infection suppressed the protein expression of Lamp1, Lamp2A, and CTSD. However, in the presence of LPS treatment, *capn1* knockout promoted the expression of these proteins. Importantly, this promoting effect was reversed upon PAK treatment (Fig. 3g). In summary, the knockout of CAPN1 can reverse the inhibitory effect of PAK infection on autolysosomes in ALI mouse lung tissues.

Effect of CAPN1 on Autophagy and Inflammatory Response in PAK-Infected TC-1 Cells

To probe into the impact of CAPN1 on autophagy and the inflammatory response in PAK-infected TC-1 cells, an in vitro model of ALI and bacterial pneumonia in TC-1 cells was established through treatment with LPS or PAK. qRT-PCR was utilized to measure the expression of *capn1* in TC-1 cells subjected to different treatments. The results revealed that only PAK treatment significantly increased the expression of *capn1* (Fig. 4a). The qRT-PCR detection results indicated that si-*capn1* was successfully transfected into TC-1 cells (transfection efficiency was 70%) (Fig. 4b). Subsequently, TC-1 cells were transfected with si-*capn1* or si-NC and were then treated with LPS or PAK. Further analysis showed that, compared to cells in the LPS+si-NC group, the expression of *capn1* was significantly reduced in the LPS+si-*capn1* group. In the PAK+si-NC group, the expression of *capn1* was markedly enhanced, while the expression of *capn1* in the PAK+si-*capn1* group was restored to control levels (Fig. 4c). Transmission electron microscopy was utilized to observe the quantity of autolysosomes in the cells, with outcomes showing that lowering CAPN1 expression increased the number of autophagosomes and autolysosomes. PAK treatment was observed to inhibit the quantity of both, and this effect was reversed when CAPN1 expression was reduced (Fig. 4d). The expression of LC3 indicated that PAK infection suppressed LC3 expression, and this effect was reversed when CAPN1 was knocked down (Fig. 4e). Detection of LC3-II and LC3-I expression revealed that PAK infection inhibited LC3-II and the LC3-II/LC3-I ratio. However, this suppression was reversed in cells with lowered CAPN1 expression (Fig. 4f). Further evaluation of Lamp1, Lamp2A, and CTSD expression in the cells showed that PAK infection led to decreased expression of these proteins. Knocking down CAPN1 reversed the inhibitory effect of PAK infection on these proteins (Fig. 4g). Finally, ELISA tests determined the levels of TNF-α, IL-1β, and IL-6 in the cell supernatant. Both LPS and PAK treatments promoted the expression of TNF-α, IL-1β, and IL-6, with PAK treatment having a more pronounced effect. Knocking down CAPN1 reversed the expression of TNF-α, IL-1β, and IL-6 (Fig. 4h). In summary, lowering CAPN1 expression can reverse the impact of PAK infection on autophagy and the inflammatory response in TC-1 cells.

CAPN1 Interacts with TFEB and Prevents It from Entering the Nucleus

To explore the relationship between CAPN1 and TFEB, we conducted a Pearson correlation analysis of *capn1* and *tfeb* and found that the expression of *capn1* and *tfeb* was negatively correlated (Fig. 5a). We hypothesized that CAPN1 might interact with TFEB. To investigate this, TC-1 cells were divided into three groups: control, PAK+si-NC, and PAK+si-*capn1*. qRT-PCR analysis was executed to ascertain the expression of *tfeb*. The results showed that PAK treatment inhibited *tfeb* expression, and further treatment with si-*capn1* restored *tfeb* expression (Fig. 5b). Co-immunoprecipitation results confirmed the interaction between CAPN1 and TFEB. PAK induction enhanced this interaction (Fig. 5c, d). The GST pull-down experiment results indicated that CAPN1 could interact well with TFEB (Fig. 5e). TFEB activity is tightly regulated by multiple mechanisms, including spatial distribution. For example, phosphorylated TFEB has no transcriptional activity when it is in the cytoplasm, but

when stimulated, it dephosphorylates into the nucleus and exerts transcriptional activity [23]. Therefore, combined with our previous studies, we hypothesized that CAPN1 might inhibit its expression by interacting with TFEB and preventing it from entering the nucleus. To verify this hypothesis, we used cellular immunofluorescence to observe the localization of TFEB in cells after CAPN1 knockdown. As shown in Figure 5f, low CAPN1 expression can promote nuclear translocation of TFEB. In addition, we performed karyoplasmic separation on TC-1 cells and detected the expression of TFEB in the nucleus by WB. The results showed that the expression level of TFEB protein in the nucleus was significantly up-regulated after transfection of si-*capn1* (Fig. 5g). In summary, CAPN1 interacted with TFEB and prevented TFEB from entering the nucleus.

TFEB's Effect on Autophagy and Inflammatory Response in PAK-Infected TC-1 Cells

Subsequently, TC-1 cells were transfected with oe-NC or oe-TFEB and treated with PAK or saline. qRT-PCR was performed to assess the expression of *tfeb* in cells. The results indicated that PAK treatment inhibited *tfeb* expression, and transfection with oe-*tfeb* followed by PAK treatment restored *tfeb* expression levels (Fig. 6a). Transmission electron microscopy was used to observe the quantity of autolysosomes in cells. It was observed that overexpression of *tfeb* reversed the inhibitory effect of PAK treatment on the quantity of autolysosomes (Fig. 6b). IF staining for LC3 expression showed that transfection with oe-*tfeb* attenuated the inhibitory effect of PAK treatment on LC3 expression (Fig. 6c). Measurement of LC3-II and LC3-I expression in cells revealed that overexpression of TFEB, in combination with PAK treatment, reversed the inhibitory effect of PAK alone on LC3-II and the LC3-II/LC3-I ratio (Fig. 6d). Furthermore, protein levels of Lamp1, Lamp2A, and CTSD were assessed in cells. The results indicated that in cells treated with PAK and oe-NC, the expression of Lamp1, Lamp2A, and CTSD was downregulated. However, in cells treated with PAK and oe-*tfeb*, the protein expression of Lamp1, Lamp2A, and CTSD was restored to control levels (Fig. 6e). Finally, ELISA was used to measure the levels of TNF-α, IL-1β, and IL-6 in the cell culture supernatant. PAK treatment promoted the expression of these inflammatory cytokines, and this effect was reversed when cells were transfected with oe-*tfeb* followed by PAK treatment (Fig. 6f). In summary, overexpression of TFEB can reverse the impact of PAK infection on autophagy and the inflammatory response in TC-1 cells.

CAPN1 Inhibits Autophagy and Promotes PAK-Induced Infection by Interacting with TFEB

To fully confirm the conclusions of this study, the following groups were constructed based on TC-1 cells: Control, PAK+oe-NC, PAK+oe-*capn1*, and PAK+oe-*capn1*+oe-*tfeb*. qRT-PCR was used to detect the mRNA expression of *capn1* and *tfeb* in the above-treated cells. It was found that PAK treatment increased *capn1* expression and inhibited *tfeb* expression; transfection with oe-*capn1* and PAK treatment resulted in higher *capn1* expression, while the expression level of *tfeb* was significantly lower than in the PAK+oe-NC group; in the PAK+oe-*capn1*+oe-*tfeb* group, *capn1* expression was similar to that of the PAK+oe-*capn1* group, but *tfeb* expression returned to the level of the PAK+oe-NC group (Fig. 7a). Transmission electron microscopy was used to observe the number of autolysosomes in cells. It was found that PAK could inhibit the number of autolysosomes in cells; transfection with oe-*capn1* and PAK treatment resulted in even fewer autolysosomes, while treatment with oe-*tfeb* could reverse the inhibitory effect of oe-*capn1* on the number of autolysosomes in cells (Fig. 7b). IF detection of LC3 expression showed that PAK could reduce LC3 expression; transfection with oe-*capn1* and PAK treatment further decreased LC3 expression, while treatment with oe-*tfeb* could reverse the inhibitory effect of oe-*capn1* on LC3 expression in cells (Fig. 7c). Detection of LC3-II and LC3-I expression in cells revealed that PAK could inhibit the expression of LC3-II and the ratio of LC3-II/LC3-I; transfection with oe-*capn1* and PAK treatment resulted in even lower expression of LC3-II and LC3-II/LC3-I ratio, while treatment with oe-*tfeb* could alleviate the inhibitory effect of oe-*capn1* on LC3-II expression and LC3-II/LC3-I ratio (Fig. 7d). Further detection of Lamp1, Lamp2A, and CTSD expression in cells showed that the expression of Lamp1, Lamp2A, and CTSD was downregulated in the PAK+oe-NC group, while the protein expression of Lamp1, Lamp2A, and CTSD was even lower in the PAK+oe-*capn1* group; in the PAK+oe-*capn1*+oe-*tfeb* group, the protein levels returned to those of the PAK+oe-NC group (Fig. 7e). Finally, ELISA was used to detect the levels of TNF-α, IL-1β, and IL-6 in the cell culture supernatant, showing that PAK treatment could promote the expression of TNF-α, IL-1β, and IL-6; transfection with oe-*capn1* and PAK treatment resulted in higher expression levels, and transfection with oe-*tfeb* inhibited the levels of inflammatory factors based on this (Fig. 7f). In conclusion, overexpression of TFEB can reverse the effects of CAPN1 overexpression on autophagy and inflammatory responses in TC-1 cells.

Discussion

P. aeruginosa is a Gram-negative rod-shaped bacterium that can cause opportunistic lung infections in susceptible individuals [24, 25]. *P. aeruginosa* is often characterized by its multi-drug resistance, and effective treatments have yet to be developed, making the management of infections caused by this bacterium particularly challenging [1, 26]. The pathogenicity of *P. aeruginosa* is the result of long-term adaptation and evolution. Pathological changes associated with *P. aeruginosa* infections include inflammatory responses, cytokine secretion, immune cell infiltration, impairment of the pulmonary blood-air barrier, leakage, and cell death [1, 27]. Previous studies have indicated that in the early stages of *P. aeruginosa* infection, there is a significant upregulation of inflammatory cytokines (TNF, CXCL1, IL-6, and IL-1β) at the site of injury in mice, along with strong neutrophil and macrophage infiltration [28]. For instance, the overexpression of BD-2 (cationic antimicrobial peptide) is shown to reduce *P. aeruginosa* levels in the lungs of ALI mice, thereby reducing neutrophil infiltration, alveolar damage, and pulmonary interstitial edema. It also inhibited the expression of ICAM-1 in lung tissues and enhanced mouse survival rates [29].

Our study demonstrated that PAK treatment promoted lung injury in mice, increasing neutrophil and macrophage infiltration and the expression of inflammatory cytokines (TNF-α, IL-1β, and IL-6), which was consistent with previous research results [28]. During severe infections, the reduction or loss of autophagy has a significant influence on lung function. Moreover, secondary bacterial infections pose a high risk in survivors of severe sepsis or trauma/hemorrhage, due to immune suppression [30]. For example, after CLP-induced ALI in mice, intraperitoneal injection of the autophagy inducer rapamycin promoted the expression of LC3-II, Beclin 1, LAMP2, and Rab7, increasing mouse survival rates. This revealed the involvement of autophagy activation in the pathological processes of sepsis-related ALI, alleviating the excessive release of inflammatory factors and lung injury [31]. Ouyang et al. [32] demonstrated that ZKSCAN3-dependent autolysosomes and lysosomal depletion may weaken lung injury recovery, triggering complications after sepsis, including organ fibrosis. Similarly, our study also indicated that PAK infection can suppress the expression of autolysosome-related proteins. This exacerbated ALI by inhibiting the ALP. In summary, these research findings underscored the significance of the ALP in the pathogenesis of ALI, providing potential therapeutic targets for the treatment of ALI.

This study provided evidence of CAPN1 expression and its role in suppressing the ALP in a bacterial lung infection model. The research demonstrated that CAPN1 accumulates in the lungs following severe bacterial pneumonia. CAPN1-deficient (*capn1*−/−) mice showed an increase in the number of lysosomes in the lung tissue, promoting the expression of autophagy and lysosome-related proteins. Importantly, *capn1*−/− mice exhibited improved outcomes in PAK-induced ALI compared to wild-type mice. Cellular models further confirm that knocking down CAPN1 can suppress the effects of PAK infection on autophagy and inflammatory responses in TC-1 cells. These findings were consistent with previous research indicating that genetic or pharmacological inhibition of CAPN1 can enhance lysosomal function, thereby ameliorating the ALP and mitigating neuronal damage in the context of cerebral ischemia [20]. This study further supported the role of CAPN1 in the ALP, suggesting that targeting CAPN1 may be a potential strategy for the treatment of ALI.

Additionally, bioinformatics analysis and co-immunoprecipitation experiments revealed a negative correlation between CAPN1 and TFEB expression. Moreover, IF staining confirmed that low expression of CAPN1 could promote nuclear translocation of TFEB and protein expression in the nucleus so we speculated that CAPN1 might interact with TFEB to form a heterodimer, thus preventing TFEB from entering the nucleus. TFEB is a master regulator of lysosomal and autophagic pathways, governing the expression of genes involved in lysosome biogenesis, and regulating the coordinated lysosomal expression and regulation network. TFEB promotes the expression of various autophagy and lysosome-related genes, including LC3 and LAMP1 [22, 33, 34]. Prior studies have highlighted that the TFEB-mediated ALP is a mechanism to ameliorate pathological changes associated with myocardial ischemia and neurodegenerative diseases. For example, TFEB levels decrease gradually in the late stages of ischemia, coinciding with reduced lysosomal activity, autophagosome accumulation, and exacerbation of ischemic damage [35]. In the context of PAK infection, TFEB levels are reduced in mouse lung tissue, and the expression of LAMP1 and LC3-II proteins is suppressed [32]. Consistent with previous research, this study showed that PAK infection in mice results in decreased TFEB levels in lung tissue homogenates, as well as downregulation of autophagy-lysosome-related proteins (LC3-II, LC3-I, LAMP1, LAMP2A, and CTSD) and inflammatory cytokines (TNF-α, IL-1β, IL-6). The results confirmed the crucial role of TFEB in the ALP and further elucidated its mediating role in the pathogenesis of PAK-induced ALI. In conclusion, this work emphasized the potential therapeutic relevance of targeting CAPN1 and TFEB in the management

of ALI and provided valuable insights into the molecular mechanisms underlying autophagy-lysosome dysregulation in the context of bacterial lung infections.

Here, we provided new evidence demonstrating the impact of CAPN1 in mediating the ALP in PAK-infected mice with ALI. Additionally, we showed that CAPN1 can interact with TFEB and that either knocking down CAPN1 or overexpressing TFEB can mediate the suppression of the ALP in PAK-induced lung injury. However, limitations exist as the expression of CAPN1 and TFEB has not been validated at the clinical level. Furthermore, the mechanisms underlying CAPN1 expression in PAK-induced ALI remain to be elucidated. Therefore, further investigations are warranted. In summary, our research provided new insights into CAPN1 and TFEB as novel targets for the management of ALI.

Statement of Ethics

This study protocol was reviewed and approved by the Experimental Animal Ethics Committee of Lishui University School of Medicine, Approval No. 2023YD0110.

Conflict of Interest Statement

The authors have no conflicts of interest to declare.

Funding Sources

This research received no specific grant from any funding agency in the public, commercial, or not for profit sectors.

Author Contributions

Conception and design: Yueming Wu and Miaomiao Chen. Provision of study materials: Hua Chen and Liuhua Pan. Collection and assembly of data: Jing Zhao and Shunnan Sun. Data analysis and manuscript writing: Junlong Xu and Ning Zhang. Final approval of manuscript: all authors.

Data Availability Statement

The data that support the findings of this study are not publicly available due to privacy but are available from the corresponding author upon reasonable request.

References

1 Deshpande R, Zou C. Pseudomonas aeruginosa induced cell death in acute lung injury and acute respiratory distress syndrome. Int J Mol Sci. 2020;21(15):5356. https://doi.org/10.3390/ijms21155356

2 Sawa T. The molecular mechanism of acute lung injury caused by Pseudomonas aeruginosa: from bacterial pathogenesis to host response. J Intensive Care. 2014;2(1):10. https://doi.org/10.1186/2052-0492-2-10

3 Sung PS, Peng YC, Yang SP, Chiu CH, Hsieh SL. CLEC5A is critical in Pseudomonas aeruginosa-induced NET formation and acute lung injury. JCI Insight. 2022;7(18):e156613. https://doi.org/10.1172/jci.insight.156613

4 Chambers ED, White A, Vang A, Wang Z, Ayala A, Weng T, et al. Blockade of equilibrative nucleoside transporter 1/2 protects against Pseudomonas aeruginosa-induced acute lung injury and NLRP3 inflammasome activation. FASEB J. 2020;34(1):1516–31. https://doi.org/10.1096/fj.201902286R

5 Liu C, Xiao K, Xie L. Advances in the use of exosomes for the treatment of ALI/ARDS. Front Immunol. 2022;13:971189. https://doi.org/10.3389/fimmu.2022.971189

6 Qu L, Chen C, Chen Y, Li Y, Tang F, Huang H, et al. High-Mobility Group Box 1 (HMGB1) and autophagy in Acute Lung Injury (ALI): a review. Med Sci Monit. 2019;25:1828–37. https://doi.org/10.12659/MSM.912867

7 Nowosad A, Jeannot P, Callot C, Creff J, Perchey RT, Joffre C, et al. p27 controls Ragulator and mTOR activity in amino acid-deprived cells to regulate the autophagy-lysosomal pathway and coordinate cell cycle and cell growth. Nat Cell Biol. 2020;22(9):1076–90. https://doi.org/10.1038/s41556-020-0554-4

8 Baxt LA, Garza-Mayers AC, Goldberg MB. Bacterial subversion of host innate immune pathways. Science. 2013;340(6133):697–701. https://doi.org/10.1126/science.1235771

9 Ryter SW, Choi AM. Autophagy in lung disease pathogenesis and therapeutics. Redox Biol. 2015;4:215–25. https://doi.org/10.1016/j.redox.2014.12.010

10 Zhang D, Li C, Zhou J, Song Y, Fang X, Ou J, et al. Autophagy protects against ischemia/reperfusion-induced lung injury through alleviating blood-air barrier damage. J Heart Lung Transplant. 2015;34(5):746–55. https://doi.org/10.1016/j.healun.2014.12.008

11 Ceelen JJM, Schols A, van Hoof SJ, de Theije CC, Verhaegen F, Langen RCJ. Differential regulation of muscle protein turnover in response to emphysema and acute pulmonary inflammation. Respir Res. 2017;18(1):75. https://doi.org/10.1186/s12931-017-0531-z

12 Sorimachi H, Hata S, Ono Y. Calpain chronicle: an enzyme family under multidisciplinary characterization. Proc Jpn Acad Ser B Phys Biol Sci. 2011;87(6):287–327. https://doi.org/10.2183/pjab.87.287

13 Kuchay SM, Chishti AH. Calpain-mediated regulation of platelet signaling pathways. Curr Opin Hematol. 2007;14(3):249–54. https://doi.org/10.1097/MOH.0b013e3280ef68f8

14 Kakurina GV, Kolegova ES, Shashova EE, Cheremisina OV, Choynzonov EL, Kondakova IV. Relationship between the mRNA expression levels of calpains 1/2 and proteins involved in cytoskeleton remodeling. Acta naturae. 2020;12(1):110–3. https://doi.org/10.32607/actanaturae.10947

15 Kling A, Jantos K, Mack H, Hornberger W, Drescher K, Nimmrich V, et al. Discovery of novel and highly selective inhibitors of calpain for the treatment of Alzheimer's disease: 2-(3-phenyl-1H-pyrazol-1-yl)-nicotinamides. J Med Chem. 2017;60(16):7123–38. https://doi.org/10.1021/acs.jmedchem.7b00731

16 Cuzzocrea S, Chatterjee PK, Mazzon E, Serraino I, Dugo L, Centorrino T, et al. Effects of calpain inhibitor I on multiple organ failure induced by zymosan in the rat. Crit Care Med. 2002;30(10):2284–94. https://doi.org/10.1097/00003246-200210000-00017

17 Hu H, Li X, Li Y, Wang L, Mehta S, Feng Q, et al. Calpain-1 induces apoptosis in pulmonary microvascular endothelial cells under septic conditions. Microvasc Res. 2009;78(1):33–9. https://doi.org/10.1016/j.mvr.2009.04.005

18 Yamashima T. Implication of cysteine proteases calpain, cathepsin and caspase in ischemic neuronal death of primates. Prog Neurobiol. 2000;62(3):273–95. https://doi.org/10.1016/s0301-0082(00)00006-x
19 Yamashima T, Tonchev AB, Tsukada T, Saido TC, Imajoh-Ohmi S, Momoi T, et al. Sustained calpain activation associated with lysosomal rupture executes necrosis of the postischemic CA1 neurons in primates. Hippocampus. 2003;13(7):791–800. https://doi.org/10.1002/hipo.10127
20 Liu Y, Che X, Zhang H, Fu X, Yao Y, Luo J, et al. CAPN1 (Calpain1)-Mediated impairment of autophagic flux contributes to cerebral ischemia-induced neuronal damage. Stroke. 2021;52(5):1809–21. https://doi.org/10.1161/STROKEAHA.120.032749
21 Qiu YW, Chen D, Xu MY, Li ST. Beneficial effects of dantrolene on sepsis-induced diaphragmatic dysfunction are associated with downregulation of high-mobility group box 1 and calpain-caspase-3 proteolytic pathway. J Surg Res. 2016;200(2):637–47. https://doi.org/10.1016/j.jss.2015.09.026
22 Füllgrabe J, Klionsky DJ, Joseph B. The return of the nucleus: transcriptional and epigenetic control of autophagy. Nat Rev Mol Cell Biol. 2014;15(1):65–74. https://doi.org/10.1038/nrm3716
23 Puertollano R, Ferguson SM, Brugarolas J, Ballabio A. The complex relationship between TFEB transcription factor phosphorylation and subcellular localization. EMBO J. 2018;37(11):e98804. https://doi.org/10.15252/embj.201798804
24 Sousa D, Justo I, Domínguez A, Manzur A, Izquierdo C, Ruiz L, et al. Community-acquired pneumonia in immunocompromised older patients: incidence, causative organisms and outcome. Clin Microbiol Infect. 2013;19(2):187–92. https://doi.org/10.1111/j.1469-0691.2012.03765.x
25 Rayees S, Joshi JC, Joshi B, Vellingiri V, Banerjee S, Mehta D. Protease-activated receptor 2 promotes clearance of Pseudomonas aeruginosa infection by inducing cAMP-Rac1 signaling in alveolar macrophages. Front Pharmacol. 2022;13:874197. https://doi.org/10.3389/fphar.2022.874197
26 Vincent JL, Rello J, Marshall J, Silva E, Anzueto A, Martin CD, et al. International study of the prevalence and outcomes of infection in intensive care units. JAMA. 2009;302(21):2323–9. https://doi.org/10.1001/jama.2009.1754
27 Coorens M, Banaschewski BJH, Baer BJ, Yamashita C, van Dijk A, Haagsman HP, et al. Killing of Pseudomonas aeruginosa by chicken cathelicidin-2 is immunogenically silent, preventing lung inflammation in vivo. Infect Immun. 2017;85(12):e00546-17. https://doi.org/10.1128/IAI.00546-17
28 Sweere JM, Ishak H, Sunkari V, Bach MS, Manasherob R, Yadava K, et al. The immune response to chronic Pseudomonas aeruginosa wound infection in immunocompetent mice. Adv Wound Care. 2020;9(2):35–47. https://doi.org/10.1089/wound.2019.1039
29 Shu Q, Shi Z, Zhao Z, Chen Z, Yao H, Chen Q, et al. Protection against Pseudomonas aeruginosa pneumonia and sepsis-induced lung injury by overexpression of beta-defensin-2 in rats. Shock. 2006;26(4):365–71. https://doi.org/10.1097/01.shk.0000224722.65929.58
30 Clarke AJ, Simon AK. Autophagy in the renewal, differentiation and homeostasis of immune cells. Nat Rev Immunol. 2019;19(3):170–83. https://doi.org/10.1038/s41577-018-0095-2
31 Zhao H, Chen H, Xiaoyin M, Yang G, Hu Y, Xie K, et al. Autophagy activation improves lung injury and inflammation in sepsis. Inflammation. 2019;42(2):426–39. https://doi.org/10.1007/s10753-018-00952-5
32 Ouyang X, Becker E Jr, Bone NB, Johnson MS, Craver J, Zong WX, et al. ZKSCAN3 in severe bacterial lung infection and sepsis-induced immunosuppression. Lab Invest. 2021;101(11):1467–74. https://doi.org/10.1038/s41374-021-00660-z
33 Sardiello M, Palmieri M, di Ronza A, Medina DL, Valenza M, Gennarino VA, et al. A gene network regulating lysosomal biogenesis and function. Science. 2009;325(5939):473–7. https://doi.org/10.1126/science.1174447
34 Settembre C, Di Malta C, Polito VA, Garcia Arencibia M, Vetrini F, Erdin S, et al. TFEB links autophagy to lysosomal biogenesis. Science. 2011;332(6036):1429–33. https://doi.org/10.1126/science.1204592
35 Liu Y, Xue X, Zhang H, Che X, Luo J, Wang P, et al. Neuronal-targeted TFEB rescues dysfunction of the autophagy-lysosomal pathway and alleviates ischemic injury in permanent cerebral ischemia. Autophagy. 2019;15(3):493–509. https://doi.org/10.1080/15548627.2018.1531196